

Multiple Fano resonances in metal-insulator-metal waveguide with umbrella resonator coupled with metal baffle for refractive index sensing

Yun-Ping Qi(祁云平), Li-Yuan Wang(王力源), Yu Zhang(张宇), Ting Zhang(张婷), Bao-He Zhang(张宝和), Xiang-Yu Deng(邓翔宇), Xiang-Xian Wang(王向贤)

Citation: Chin. Phys. B . 2020, 29(6): 067303 . **doi:** 10.1088/1674-1056/ab888c
Journal homepage: http://cpb.iphy.ac.cn; http://iopscience.iop.org/cpb

What follows is a list of articles you may be interested in

Coupling-induced spectral splitting for plasmonic sensing with ultra-high figure of merit

Hua Lu(陆华), Yi-Cun Fan(范奕村), Si-Qing Dai(戴思清), Dong Mao(毛东), Fa-Jun Xiao(肖发俊), Peng Li(李鹏), Jian-Lin Zhao(赵建林)

Chin. Phys. B . 2018, 27(11): 117302 . **doi:** 10.1088/1674-1056/27/11/117302

Gap plasmon-enhanced photoluminescence of monolayer MoS_2 in hybrid nanostructure

Le Yu(余乐), Di Liu(刘頔), Xiao-Zhuo Qi(祁晓卓), Xiao Xiong(熊霄), Lan-Tian Feng(冯兰天), Ming Li(李明), Guo-Ping Guo(郭国平), Guang-Can Guo(郭光灿), Xi-Feng Ren(任希锋)

Chin. Phys. B . 2018, 27(4): 047302 . **doi:** 10.1088/1674-1056/27/4/047302

Thermal emission properties of one-dimensional grating with different parameters

Weixin Lin(林伟新), Guozhou Li(李国洲), Qiang Li(李强), Hongjin Hu(胡宏锦), Fang Han(韩防), Fanwei Zhang(张樊伟), Lijun Wu(吴立军)

Chin. Phys. B . 2017, 26(5): 057301 . **doi:** 10.1088/1674-1056/26/5/057301

Coherent and tunable radiation with power enhancement from surface plasmon polaritons

Gong Sen, Zhong Ren-Bin, Hu Min, Chen Xiao-Xing, Zhang Ping, Zhao Tao, Liu Sheng-Gang

Chin. Phys. B . 2015, 24(7): 077302 . **doi:** 10.1088/1674-1056/24/7/077302

Rainbow trapping based on long-range plasmonic Bragg gratings at telecom frequencies

Chen Lin, Zhang Tian, Li Xun

Chin. Phys. B . 2013, 22(7): 077301 . **doi:** 10.1088/1674-1056/22/7/077301

Multiple Fano resonances in metal–insulator–metal waveguide with umbrella resonator coupled with metal baffle for refractive index sensing*

Yun-Ping Qi(祁云平)[1,3,†], Li-Yuan Wang(王力源)[1], Yu Zhang(张宇)[1], Ting Zhang(张婷)[1], Bao-He Zhang(张宝和)[1], Xiang-Yu Deng(邓翔宇)[1], and Xiang-Xian Wang(王向贤)[2]

[1] *College of Physics and Electronic Engineering, Northwest Normal University, Lanzhou* 730070, *China*
[2] *School of Science, Lanzhou University of Technology, Lanzhou* 730050, *China*
[3] *Engineering Research Center of Gansu Provence for Intelligent Information Technology and Application, Northwest Normal University, Lanzhou* 730070, *China*

(Received 19 January 2020; revised manuscript received 2 April 2020; accepted manuscript online 12 April 2020)

A single baffle metal–insulator–metal (MIM) waveguide coupled with a semi-circular cavity and a cross-shaped cavity is proposed based on the multiple Fano resonance characteristics of surface plasmon polaritons (SPPs) subwavelength structure. The isolated state formed by two resonators interferes with the wider continuous state mode formed by the metal baffle, forming Fano resonance that can independently be tuned into five different modes. The formation mechanism of Fano resonance is analyzed based on the multimode interference coupled mode theory (MICMT). The finite element method (FEM) and MICMT are used to simulate the transmission spectra of this structure and analyze the influence of structural parameters on the refractive index sensing characteristics. And the transmission responses calculated by the FEM simulation are consistent with the MICMT theoretical results very well. The results show that the figure of merit (FOM) can reach 193 and the ultra-high sensitivity is 1600 nm/RIU after the structure parameters have been optimized, and can provide theoretical basis for designing the high sensitive refractive index sensors based on SPPs waveguide for high-density photonic integration with excellent performance in the near future.

Keywords: surface plasmon polaritons, MIM waveguide, Fano resonance, finite element method

PACS: 73.20.Mf, 42.79.–e, 71.36.+c, 71.38.–k **DOI:** 10.1088/1674-1056/ab888c

1. Introduction

Surface plasmon polaritons (SPPs) are a kind of collective oscillation caused by the interaction between electromagnetic wave and free electrons on the metal surface. The SPPs can overcome the diffraction limit and confine light in subwavelength dimension, so it very promises to be used as an information carrier for high-density photonic integration circuits. The metal–insulator–metal (MIM) waveguide has strong binding ability to serve as SPPs with low transmission loss and bending loss, small structure size, long transmission distance, and many other characteristics, and it can realize the manipulation of nanoscale light. Therefore, the MIM waveguide is one of the most promising waveguide structures for realizing nano optical equipment and highly integrated nano optical circuits. Recently, Fano resonance has received attention of many researchers and has been realized in many systems. Moreover, the Fano resonance effect generated in the MIM waveguide structure is particularly sensitive to environmental change. Meanwhile, the Fano resonance, a sharp asymmetric line-shape, can be induced by changing the MIM waveguide structure, through which the higher quality factors and sensitivity than traditional Lorentz resonance can be achieved. The Fano resonance was found first in the autoionized state of atoms, and then in classical optical systems.[1] Ugo Fano pointed out that the interference between a wide continuum state and a narrow discrete state can give rise to asymmetric peaks in transmission spectra. Fano gave this phenomenon an earlier qualitative explanation.[1] This theory can also be extended to the interaction of one discrete level with two or more continua. Klimov *et al.*[2] verified the existence of Fano resonance by studying the optical characteristics of photonic crystals covered by perforated metal membrane, and proposed a method of designing a Fano resonance sensor sensitive to change in environmental refractive index. Klimov *et al.*'s experimental description of photonic crystals covered with perforated metal films provided a foreshadow for the research in this paper. Various MIM waveguide structures based on Fano resonance have been designed and manufactured, including optical multiplexer,[3,4] filter,[5] optical switch,[6] distributed Bragg reflector mirror,[7–9] which have the huge application prospect in biosensing technique, nano lithography,[10] and other fields. At the same time, other laboratory also conducted some researches of the applica-

*Project supported by the National Natural Science Foundation of China (Grant Nos. 61367005 and 61865008) and the Natural Science Foundation of Gansu Province, China (Grant No. 17JR5RA078).

†Corresponding author. E-mail: yunpqi@126.com

© 2020 Chinese Physical Society and IOP Publishing Ltd

tions of MIM waveguide absorbers,[11] perfect metamaterial absorber,[12–15] surface-enhanced Raman pectroscopy[16] and graphene plasmon-enhanced infrared spectroscopy.[17]

With the development of nanotechnology, on-chip high-sensitivity detection technology will become an important research direction for future sensors.[18] In Ref. [19], it was pointed out that the symmetry breaking introduced by an adjacent infinite dielectric can cause the plasmon modes of a metallic nanostructure to couple and hybridize. This effect is particularly large for entities with a large contact area adjacent to the dielectric. We can make transverse magnetic (TM) wave enter into the MIM waveguide structure, the SPPs will be generated at the MIM interface, the SPPs are a kind of collective oscillation caused by the interaction between electromagnetic waves and free electrons on the metal surface. In this way we can avoid adjacent entities with large contact areas of the dielectric. Due to the unique properties of Fano resonance and SPPs, the design of highly sensitive on-chip SPPs sensor that can be easily integrated with the help of these optical phenomena has become a research hotspot.[20] Wen *et al.*[21] proposed an MIM waveguide structure composed of a single baffle and a rectangular cavity, and studied the dual Fano resonance characteristics of the structure. The research showed that the multi Fano resonance system possesses important applications in nonlinear, slow-light, and bio-nanometer sensing devices. Wu *et al.*[22] proposed an MIM straight waveguide structure with branch nodes, studied and analyzed the effects of coupling spacing, geometric dimensions, and other parameters on Fano resonance peak. The results showed that the Fano resonance generated by this structure can be used to fabricate high precision sensors. Wu *et al.*[23] designed a kind of MIM waveguide-coupled circular ring and disc cavity structure, through continuously adding a section, which can be tuned to achieve independence in multiple Fano resonance. By changing the length of the section, the degree to which the multiple Fano resonance peaks varies is different from the single Fano peak does, because of the parallel processing ability of the multiple Fano resonance compared with that of the single Fano resonance. This structure had unique advantages in spectrometer and enhanced biochemical sensing.[24,25] The existing research on cavity mainly focused on the rule of the rectangular cavity or ring cavity, in addition, in the above studies, the position of the resonance peak needs adjusting by changing a certain parameter of the resonant cavity structure and the proposed structure was difficult to adapt to the existing level of manufacturing technology. So we design a structure which can realize the coarse modulation of the resonance peak position, the resonance peak can be independently adjust and easy to manufacture. Therefore, it will be widely used in the field of nano-refractive index sensing.[26]

In this paper, an MIM waveguide with a single metal baffle coupled with a semi-annular cavity and a cross-shaped cavity is designed. It is different from a square-shaped cavity which is easy to manufacture and study.[27] It can obtain more resonance peaks (finally, we obtain six resonance peaks). When the TM wave is incident into the MIM waveguide structure, the SPPs will be generated at the MIM interface, continuous states will be formed through the direct waveguide into the semi-annular cavity, and discrete states will be formed in the crosswise cavity. These continuous state and the discrete state are coupled to each other to form Fano resonance under the action of near field, forming five Fano resonances and one Lorentz peak. The transmission characteristics of Fano resonance formed by the coupling of the continuous state and the discrete state are analyzed by combining the multimode interference coupled mode theory (MICMT). The COMSOL software based on the finite element method (FEM) is used to simulate the structure, quantitatively analyze the influence of structural parameters on the sensing characteristics, refractive index sensitivity and FOM value, and then optimize the structural parameters, to realize the regulation of structural sensing characteristics and finally realize the multi-function and high-sensitivity sensor.[28,29]

2. Theoretical analysis

In order to discuss the structure of a single baffle MIM waveguide coupled with a semi-circular cavity and a cross-shaped cavity, we start with a single exit waveguide resonant cavity system. The resonance mode can be fully described by only the equation which is satisfied by the mode amplitude of the isolated lossless resonator system obtained as follows:[30]

$$\frac{\mathrm{d}a}{\mathrm{d}t} = -\mathrm{j}\omega_0 a, \tag{1}$$

where ω_0 is the resonance angular frequency. If the system is lossy and the loss is small, the perturbation term can be added to the mode amplitude equation to represent the loss as follows:[30]

$$\frac{\mathrm{d}a}{\mathrm{d}t} = -\mathrm{j}\omega_0 a - \frac{1}{\tau_0} a, \tag{2}$$

where $1/\tau_0$ is the attenuation rate due to the internal losses of the system and τ_0 is the decay time of internal loss of the resonant mode in resonant cavity. For the SPPs' system, a common resonant cavity or other form of perturbation of the resonant mode is the connection of the resonator to the transmission waveguide. In this case, the attenuation rate of the mode will change because the power will not only dissipate internally but also enter the waveguide. Equation (2) is further rewriten as follows:

$$\frac{\mathrm{d}a}{\mathrm{d}t} = -\mathrm{j}\omega_0 a - \left(\frac{1}{\tau_0} + \frac{1}{\tau_\mathrm{e}}\right) a, \tag{3}$$

where $1/\tau_e$ is the additional attenuation rate due to the power escaping from the resonator into the waveguide and τ_e is the decay time of the coupling between the resonant cavity and waveguide. When the waveguide carries an amplitude of s_+ and when the wave propagates to the resonant cavity, the mode amplitude a will be driven by the incident wave, then

$$\frac{da}{dt} = -j\omega_0 a - \left(\frac{1}{\tau_0} + \frac{1}{\tau_e}\right) a + \kappa s_+, \tag{4}$$

where κ means the coefficient of coupling degree between the resonant cavity and incident wave s_+, and s_+ is normalized (equal to the power of the incident wave). According to the time reversibility of Maxwell's equations, we can obtain

$$\kappa = \sqrt{\frac{2}{\tau_e}} e^{j\theta}. \tag{5}$$

The reflected wave is denoted as s_-. In a linear system, the reflected wave s_- increase or decreases as incident wave s_+ and the mode amplitude a increases or decreases, respectively, as expressed below:

$$s_- = -s_+ + \kappa^* a. \tag{6}$$

Equation (4) and the above equation (6) are the basic equations of a resonant cavity coupled to an input port (waveguide or optical mode) known as coupled mode theory (CMT).

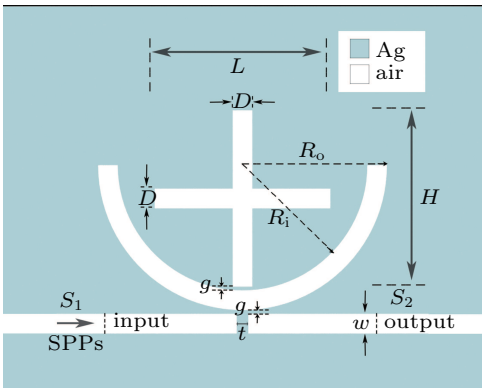


Fig. 1. Schematic diagram of umbrella resonator coupled with MIM waveguide with metal baffle.

As shown in Fig. 1, an air-filled busbar waveguide is placed on the silver metal but is cut off by the middle baffle. There are a side-coupled semi-ring cavity with an upward opening (denoted as cavity USR) above the baffle and a vertical cross structure (denoted as cavity VCS) above the side-coupled semi-ring cavity. The grey region of the proposed structure represents the relative permittivity of Ag (ε_m) represented by the Drude model and ε_m is expressed as

$$\varepsilon_m = \varepsilon_\infty - \frac{\omega_p^2}{\omega^2 + i\omega\gamma}. \tag{7}$$

The parameters in this well-known equation are set to be $\varepsilon_\infty = 3.7$, $\omega_p = 9.1$ eV, and $\gamma = 0.018$ eV.[31,32] The white part in Fig. 1 represents the insulator in the embedded waveguide and resonator is air ($\varepsilon_i = 1.0$). In this paper, the width of waveguide is fixed at $w = 50$ nm, so that only fundamental transverse magnetic wave (TM_0) is the excited spectra in the SPPs. Accordingly, we can determine that the dispersion equation of SPPs' propagation in MIM structure is[33]

$$\varepsilon_m k_i \tanh\left(-\frac{jk_i w}{2}\right) + \varepsilon_i k_m = 0. \tag{8}$$

Here, the transverse propagation constant in air and Ag can be expressed by the following equation:

$$k_{i,m} = \frac{2\pi}{\lambda}\sqrt{\varepsilon_{i,m} - 1/n_{\text{eff}}^2}.$$

On a nanoscale, the contribution of its imaginary part $\text{Im}(n_{\text{eff}})$ can be ignored, so we should pay more attention to the relative phase of the contribution of the real part $\text{Re}(n_{\text{eff}})$. Based on the standing wave theory, the resonant wavelength of the resonant cavity can be described by the following equation:[34,35]

$$\lambda = \frac{2\text{Re}(n_{\text{eff}})\, l_{\text{USR}}}{n - \phi/2\pi}, \quad n = 1, 2, 3, \ldots, \tag{9}$$

where l_{USR} represents the perimeter of the USR resonator and ϕ denotes the phase shift reflected on both ends of the resonant cavity. This relationship of two variables between λ and l_{USR} can enlighten us to design a resonant cavity with an appropriate size to achieve sharp and asymmetric Fano resonance. In the structure, the coupling phases and moduli of different resonance modes should be considered. Due to the interference between the modes, the transmittance of the plasmon system will be affected by these coupling phases φ_{n1}, φ_{n2}, so the relationship between the coupling phases needs considering. The multi-mode interference coupling theory (MICMT)[36] equations of resonant cavity and dual waveguide coupling system with phase are as follows:

$$\begin{cases} \dfrac{da_n}{dt} = -j\omega_n a_n - \left(\dfrac{1}{\tau_{n0}} + \dfrac{1}{\tau_{ne1}} + \dfrac{1}{\tau_{ne2}}\right) a_n \\ \qquad + \kappa_{n1} s_{1+} + \kappa_{n2} s_{2+}, \\ s_{1-} = -s_{1+} + \sum\limits_n \kappa_{n1}^* a_n \gamma_{n1} e^{j\varphi_{n1}}, \\ s_{2-} = -s_{2+} + \sum\limits_n \kappa_{n2}^* a_n \gamma_{n2} e^{j\varphi_{n2}}, \\ \kappa_{n1} = \sqrt{\dfrac{2}{\tau_{ne1}}} e^{j\theta_{n1}}, \quad \kappa_{n2} = \sqrt{\dfrac{2}{\tau_{ne2}}} e^{j(\theta_{n2} - \phi_n)}, \end{cases} \tag{10}$$

where $s_{1\pm}$ and $s_{2\pm}$ are the mode amplitude of the input port S_1 and output port S_2 of the waveguide incoming(corresponding to sign "+") and escaping (corresponding to sign "−") from the resonator, respectively; a_n and ω_n represent the amplitude and resonance frequency of the n-th resonance mode, respectively; τ_{n0} means the internal loss time for the n-th mode; τ_{ne1} and τ_{ne2} are the coupling attenuation time between the resonant cavity and the input/output waveguides, respectively; likewise, θ_{n1} and θ_{n2} represent coupling phases of the n-th resonant mode; ϕ_n refers to the phase difference between the

output and input ports; γ is the normalized coefficient(in this paper, $\gamma_{n1} = \gamma_{n2} \approx 1$). When the SPPs are incident only from the input port, we can assume that $s_{2+} = 0$. In this case, the complex amplitude transmission coefficient of the whole system can be expressed as

$$t = \frac{s_{2-}}{s_{1+}} = \sum_n \frac{\gamma_{n1} |\kappa_{n1}| |\kappa_{n2}| \, \mathrm{e}^{\mathrm{j}\varphi_n}}{-\mathrm{j}(\omega - \omega_n) + 1/\tau_n + 1/\tau_{\mathrm{ne1}} + 1/\tau_{\mathrm{ne2}}},$$
$$\varphi_n = \varphi_{n1} + \phi_n + \theta_{n1} - \theta_{n2}, \tag{11}$$

where φ_n is the total coupling phase of the n-th resonant mode.[37] The transmittance from the input port to the output port can be expressed by the expression $T = |t|^2$. We assume that the left part and the right part of the waveguide in the system have the same length, then we can take $\tau_{\mathrm{ne1}} = \tau_{\mathrm{ne2}} = \tau_{\mathrm{ne}}$ and $\theta_{n1} = \theta_{n2}$, and the transmittance formula of the whole system can be further simplified into

$$T = |t|^2 = \left| \sum_n \frac{2\,\mathrm{e}^{\mathrm{j}\varphi_n}}{-\mathrm{j}(\omega - \omega_n)\,\tau_{\mathrm{ne}} + 2 + \tau_{\mathrm{ne}}/\tau_n} \right|^2,$$
$$\varphi_n = \varphi_{n1} + \phi_n. \tag{12}$$

3. Simulation and discussion

3.1. Umbrella resonator coupling MIM waveguide structure with metal baffle

In the simulation of this paper, the geometric parameters of the structure are set to be as follows: waveguide width $w = 50$ nm, baffle width $t = 30$ nm, coupling distance $g = 10$ nm, vertical chamber length $H = 450$ nm, horizontal chamber length $L = 450$ nm, waveguide width of VCS $D = 50$ nm, outer circle radius $R_{\mathrm{o}} = 370$ nm, and inner circle radius $R_{\mathrm{i}} = 320$ nm. Throughout the paper, the normalized transmittance of waveguide structures is defined as the quotient of the power flow between output port S_2 and input port S_1 (acquired by integrating the Poynting vector over the MIM waveguide cross section). In addition, the transmission responses of the structure is calculated by the MICMT method and FEM simulation as shown in Fig. 2(a). The results show that the results from the MICMT (the red circle line) agree very well with the FEM simulation results (the blue solid line). The transmission spectra of the only metal baffle, only USR, VCS and the whole coupled system are shown in Fig. 2(b). For the MIM waveguides with metal baffle, the transmittance is less than 8.6% in a range of 500 nm–2000 nm.[38,39] Therefore, metal baffle can be regarded as a continuous state. To create a discrete state, a semi-annular cavity is laterally coupled to the MIM waveguide, plus a cross-shaped waveguide coupled to the semi-annular waveguide. It can be seen that there are five peaks representing the first, second, third, fourth, and fifth eigenmodes of the semi-annular cavity in a range of 500 nm–2000 nm. These five narrow resonance modes overlap with the wide continuous state, thus forming four sharp and asymmetrical Fano resonance peaks and one Lorentz peak in the transmission spectrum. These four Fano resonance peaks are FR1, FR2, FR3, and FR4, respectively, the Lorentz resonance peak is LR. For the FR1 peak at a wavelength of 555 nm the transmission rate is about 75.6%; for the FR2 peak at a wavelength of 805 nm, the transmission rate is about 67.0%; for the FR3 peak at a wavelength of 1039 nm, the transmittance rate is about 16.1%; for the FR4 peak at a wavelength of 1337 nm, the transmittance rate is about 11.9%; for LR peak at a wavelength of 1625 nm, the transmission rate is about 39.8%.

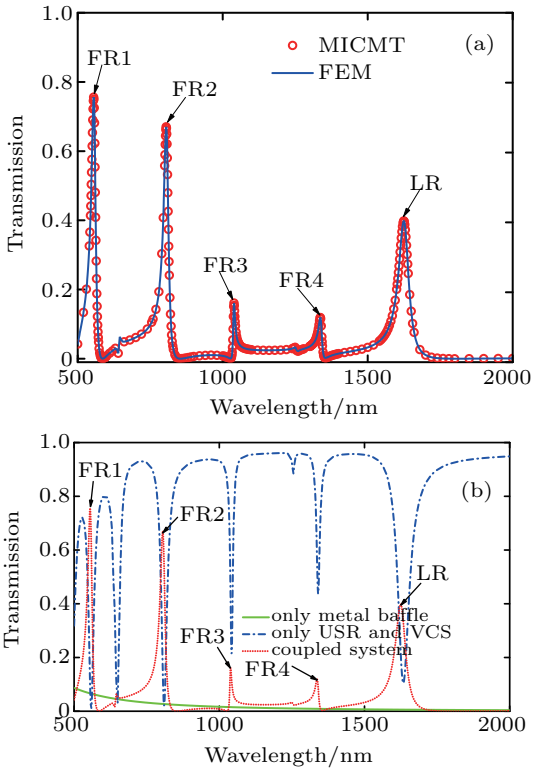


Fig. 2. (a) Transmission *versus* wavelength of the structure calculated by FEM method (blue solid line) and MICMT method (red circle), and (b) transmission *versus* wavelength of the proposed structure with only metal baffle (green solid line), only USR & VCS (blue dash–dot line), and coupled system (red dotted line) studied by COMSOL(FEM) simulation.

To better understand the physical significance of Fano resonance, figure 3 shows the magnetic field distributions of $|H_z|$ at the wavelengths of five transmission peaks (555 nm, 805 nm, 1039 nm, 1337 nm, and 1625 nm) and five transmission dips (586 nm, 854 nm, 1116.5 nm, 1354.5 nm, and 1701 nm). For the sake of research, all field profiles are normalized and the values of the color bars are unified. It can be seen from Figs. 3(a) and 3(c) that the SPPs can pass through the bus waveguide. The fairly strong magnetic field is confined into the semi-ring cavity. The distributions of the magnetic field at dip wavelength are shown in Figs. 3(b) and 3(d). We can obtain that the field in the semicircle ring resonator and waveguide has destructive interference, and most of the input energy cannot reach the outlet.[40] Further investigation

of the origin of the other two Fano resonances shows that the $|H_z|$ field distribution of FR3 and FR4 peak wavelengths at 1039 nm and 1337 nm are shown in Figs. 3(e) and 3(g), respectively. The wavelength at 1116.5 nm of FR3 dip and 1354.5 nm of FR4 dip are shown in Figs. 3(h) and 3(i), respectively. In Figs. 3(e) and 3(g), there are obvious strong field distributions in the resonator composed of USR and the metal baffle waveguide, while there are almost no SPPs waves in the VCS, which is due to the high reflectivity of the short intercept resonator. In this case, there is only a similar structure to those proposed by Chen *et al.*,[41] which are also described in Figs. 3(e) and 3(g). It can be seen from Figs. 3(h) and 3(i) that as the incident wavelength is satisfied with Eqs. (12), a standing wave in USR forms in the cavity, and the SPPs can serve as a high metal baffle reflector waveguide of reflection waveform with high quality.[42]

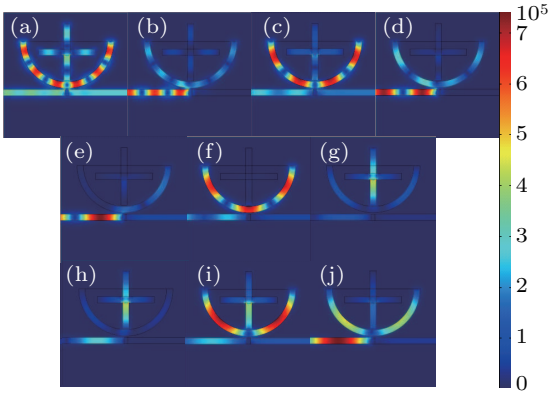


Fig. 3. Magnetic field distributions at wavelengths of five transmission peaks: (a) 555 nm, (c) 805 nm, (e) 1039 nm, (g) 1337 nm, (i) 1625 nm and of five transmission dips (b) 586 nm, (d) 854 nm, (f) 1116.5 nm, (h) 1354.5 nm, and (j) 1701 nm.

In order to make the whole system practical, considering the existing level of manufacturing technology, we analyze the effect of coupling distance g and width t of metal baffle on the performance of the whole system. First, we search the effect of the change in the lateral coupling distance g on the transmission spectrum of the whole system. As shown in Fig. 4(a), we can see that the resonance wavelength of LR shows a significant blueshift, while the resonance wavelengths of FR1, FR2, FR3, and FR4 are basically unchanged. At the same time, with the increase of the side coupling distance, the transmittance of the whole system decreases obviously. The thickening of the metal layer will certainly affect the energy exchange efficiency between the resonator and the waveguide, and thus directly affecting the transmittance of the whole system. This also means that the coupling distance g should be as small as possible in the manufacturing of the whole system. Compared with the high requirement for the coupling distance g, it can be seen from Fig. 4(b) that when the width of the metal baffle is $t = 30$ nm, there will still be no significant influence on transmittance and resonance peak wavelength.[43] So the whole performance bottleneck of our system is mainly determined by the side coupling distance g.

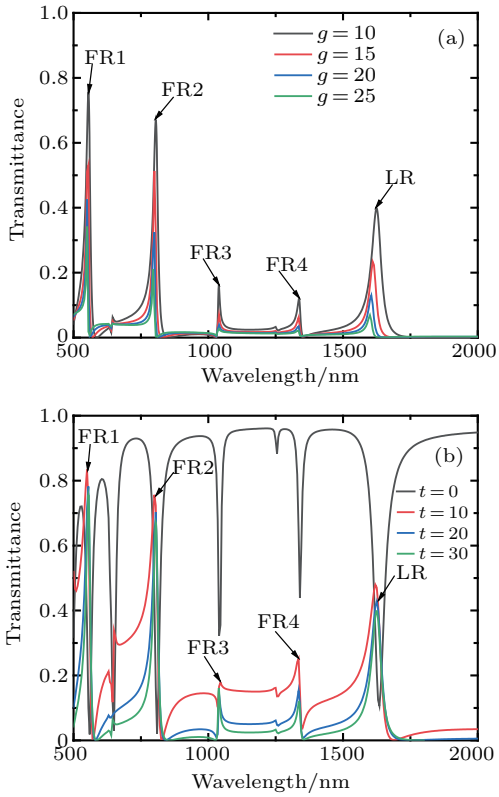


Fig. 4. Transmission spectra of MIM structure changing (a) with coupling distance g using FEM simulation, (b) with thickness of metal baffle t obtained from FEM simulation.

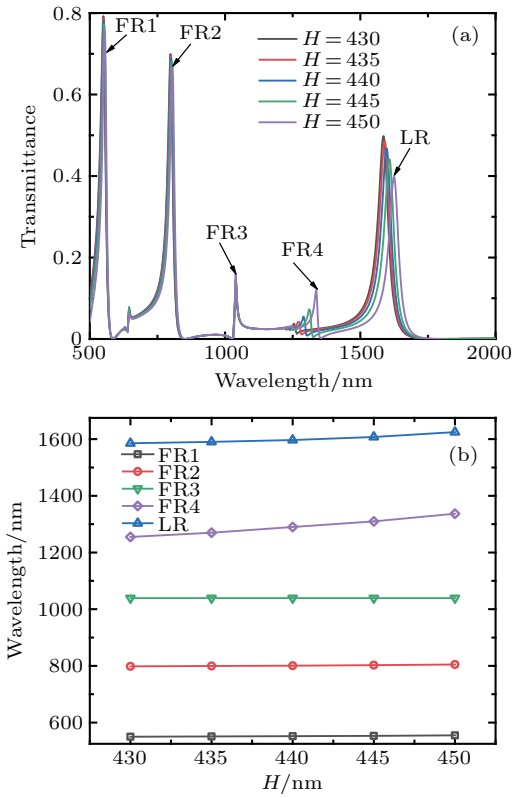


Fig. 5. (a) Transmission spectra of the system with different values of vertical cavity lengths H, and (b) resonance wavelengths of the Fano resonance peaks FR1, FR2, FR3, FR4, and Lorentz resonance peak LR changing with vertical cavity length.

We simulate the effect of the length of vertical resonator on transmission spectrum. As can be seen from Fig. 5(a), with the length of the vertical resonator H changing from 430 nm to 450 nm, the resonance peak for each of LR and FR4 presents a certain degree of redshift. We keep the length of the vertical resonator H linearly increasing, so the resonance peak in the projection spectrum also varies linearly as shown in Fig. 5(b). The length of the vertical resonator H increases linearly, the distance between the vertical resonator H and the semi-circular waveguide increases linearly, so the resonance peak also changes linearly.

Then, we change the length of the horizontal resonator L from 400 nm to 500 nm in steps of 25 nm, and the change of the transmission spectrum is shown in Fig. 6(a). As expected, only the resonance peak of FR4 is redshifted, while the other resonance peaks' positions remain unchanged. Figure 6(b) shows the changes of the resonance peaks of FR1, FR2, FR3, FR4, and LR, respectively.

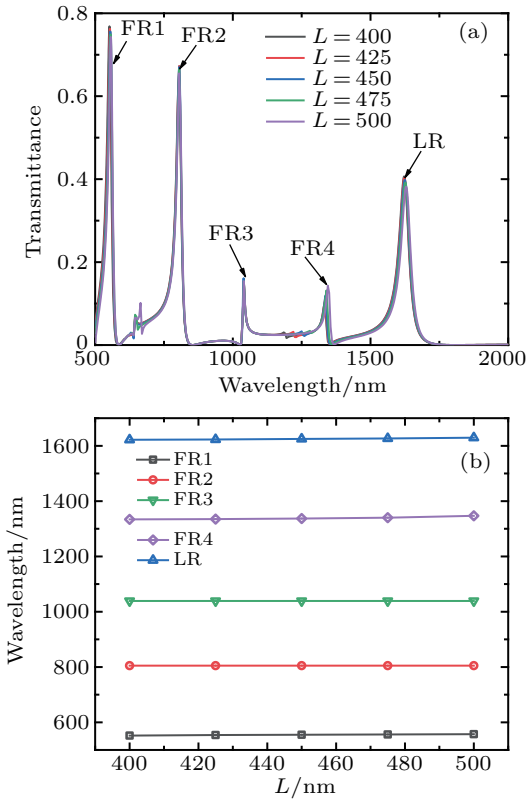


Fig. 6. (a) Transmission spectra of system with different values of horizontal cavity length L, and (b) resonance wavelengths of Fano resonance peaks FR1, FR2, FR3, FR4, and Lorentz resonance peak LR changing with horizontal cavity length L.

Because the wavelength value of the resonance peak and that of the dip of the same Fano resonance are very close to each other, our system is very excellent to make sensors. The influence of refractive index variation on transmission spectrum of the system is studied below. When we change the refractive index of the filling medium in the resonant cavity from 1.00 to 1.08 with the step 0.04, the change of the transmission spectrum is shown in Fig. 7(a). The refractive index sensitivity $S = \Delta\lambda/\Delta n$ (nm/RIU, the change of resonance peak wavelength in the transmission spectrum over the refractive index change) is used to characterize the sensor's ability to detect the change in the surrounding environment. We calculate the sensitivity of FR1, FR2, FR3, FR4, and LR to be 525 nm/RIU, 775 nm/RIU, 1025 nm/RIU, 1300 nm/RIU, 1600 nm/RIU, respectively. The maximum value of these FR sensitivity results 1300 nm/RIU and the sensitivity of LR result 1600 nm/RIU are much larger than 1100 nm/RIU in Ref. [44], 1120 nm/RIU in Ref. [45], and 900 nm/RIU in Ref. [46], respectively. This shows that the system we designed is very suitable for sensor parts. In addition, the figure of merit (FOM*) is also an important indicator for measuring the sensor performance. Generally,FOM and FOM* are defined as

$$\mathrm{FOM} = \frac{\Delta\lambda/\Delta n}{\mathrm{FWHM}} \quad \text{and} \quad \mathrm{FOM}^* = \frac{\Delta T/\Delta n}{T}, \tag{13}$$

where T is generally defined as $T = (T_{1.00} + T_{1.01})/2$ is the mean value of the system's resonance peak transmittance before and after refractive index change. Figure 7(b) shows the FOM* *versus* wavelength curve in a refractive index range from $n = 1.00$ to $n = 1.01$. From Fig. 7(b), the FOM* values of FR1, FR2, FR3, FR4, and LR, calculated from $n = 1.00$ to $n = 1.01$, are 136.70, 169.74, 133.58, 185.76, and 135.68 respectively, which are much higher than the results: 100 in Ref. [44] and 87 in Ref. [47] reported previously.

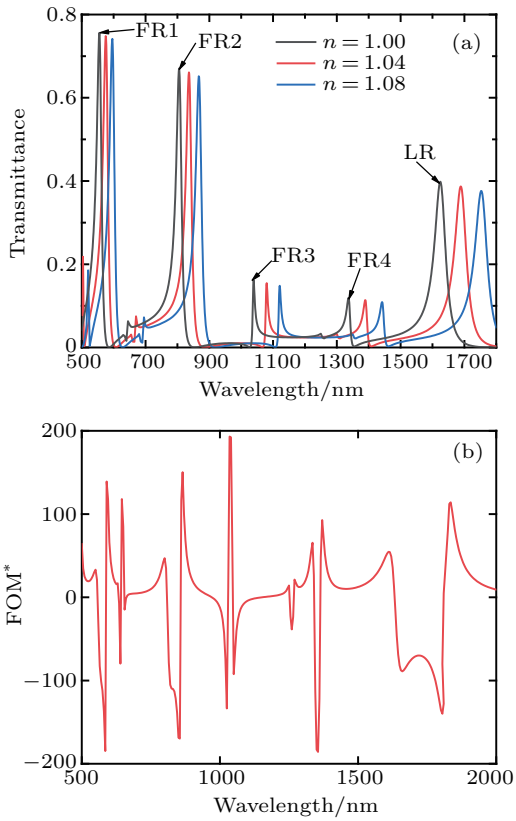


Fig. 7. (a) Transmission spectra for three different refractive indexes, and (b) FOM* varying with wavelength of the whole system.

3.2. Umbrella resonator coupling MIM waveguide structure with metal baffle (symmetry breaking)

In order to realize a chip-level integrated photonic device, multiple functions need to be performed simultaneously in a single SPPs' structure. In this case, we use the symmetry breaking method to split the horizontal resonator L of the "umbrella" refractive index sensor into L_1 and L_2, the other geometric parameters remain the same as previous ones. The umbrella resonator coupled with a metal baffle MIM waveguide symmetry-breaking structure is shown in the following Fig. 8.

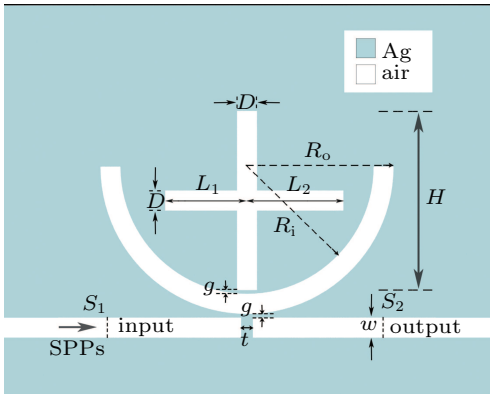


Fig. 8. Schematic diagram of umbrella resonator coupled with MIM waveguide with metal baffle (symmetry breaking).

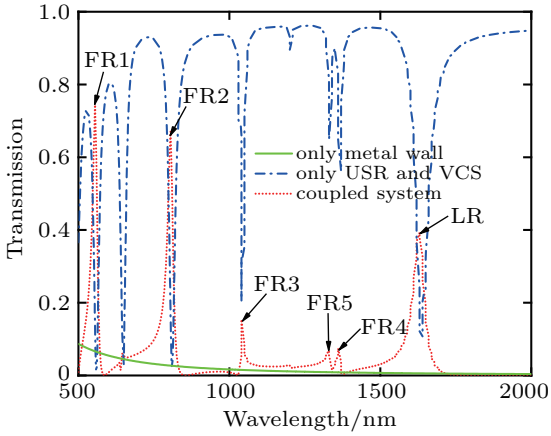


Fig. 9. COMSOL (FEM) simulated transmission spectra of proposed structures respectively with only metal baffle (green solid line), only USR & VCS (blue dash-dot line), and coupled system (red dotted line).

The transmission spectra of only metal baffle, only USR, VCS, and the whole coupled system are shown in Fig. 9. First, we discuss the change of the transmission response of the whole system before and after the symmetry breaking of the horizontal resonator. We fix the length of L_1 at 205 nm and set the degree of symmetry breaking to be $\Delta L = L_2 - L_1$, with the other parameters unchanged. When ΔL values are 30 nm, 31 nm, 35 nm, 40 nm, and 50 nm, respectively, the change of transmission spectrum is shown in Figs. 10(a) and 10(b). When $\Delta L = 31$ nm, a very weak Fano resonance that a new Fano resonance peak (FR5) gradually appears in the transmission spectrum, occurs at 1313.5 nm. When ΔL changes from 31 nm to 50 nm, the transmittance of FR5 resonance peak increases from 0.04 to 0.09, and the transmittance of dip resonance tends to 0. When the symmetry of the horizontal resonator is broken ($\Delta L = 31$ nm), the magnetic field distribution is anti-symmetric and the symmetry is further broken, Fano resonance gradually becomes stable.

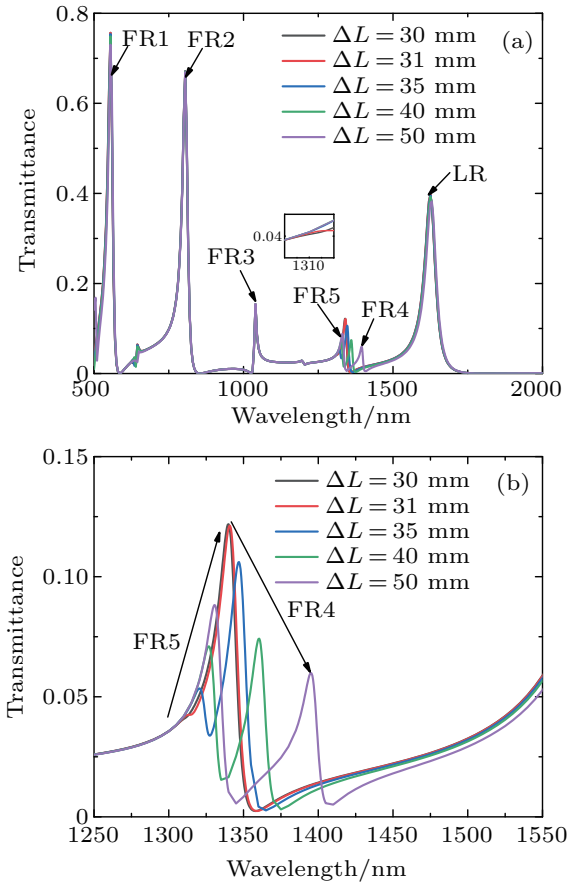


Fig. 10. Plots of transmittance *versus* wavelength of proposed system (a) before and (b) after symmetry breaking of horizontal resonant cavity for five different values of ΔL.

Figure 11 shows the magnetic field distribution of $|H_z|$ at the wavelengths of six transmission peaks. As can be seen from the figure, six sharp Fano resonances appear in the transmission spectrum, and the positions of the resonance peaks are at 555.5 nm, 805 nm, 1039 nm, 1327 nm, 1360.5 nm, and 1626 nm, respectively. We can see that FR1, FR2, and FR3 are generated by the interaction between the USR and the metal baffle, while FR4, FR5, and FR6 are generated by the interaction between USR and the VCS. We can find that the magnetic field energy values that were evenly distributed in the horizontal resonator before are different. For the FR4, the magnetic field energy is mainly concentrated in the long part of the horizontal resonator. For the FR5, the magnetic field energy is mainly concentrated in the shorter part of the horizontal resonator. The characteristic that the energy of the magnetic field is localized in different parts makes it possible to control multiple Fano resonances independently.[48]

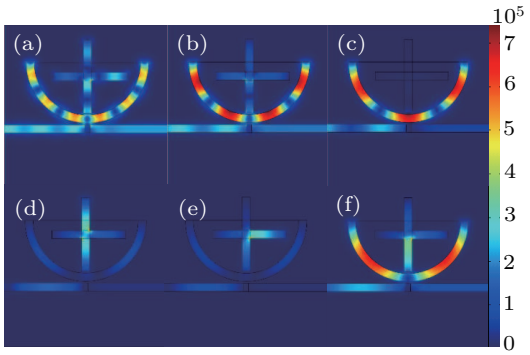


Fig. 11. Magnetic field distributions at wavelengths (a) 555.5 nm, (b) 805 nm, (c) 1039 nm, (d) 1327 nm, (e) 1360.5 nm, (f) 1626 nm, respectively.

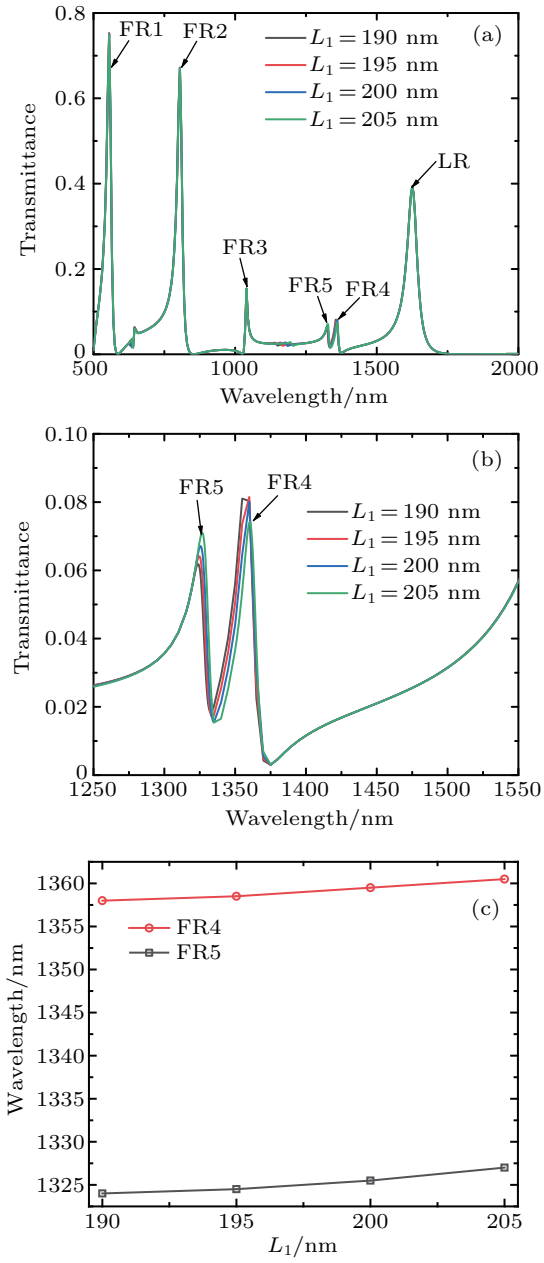


Fig. 12. (a) Transmission spectra of the MIM structure changing with length of horizontal resonator L_1, (b) transmission spectra of two Fano resonance peaks FR4 and FR5 (wavelength range from 1250 nm to 1550 nm), and (c) resonance wavelengths of the two Fano resonance peaks FR4 and FR5 changing with horizontal cavity length L_1.

We verify whether the two Fano resonances can be regulated independently by adjusting the length and the length of the horizontal resonator as shown in Figs. 12(a)–12(c). First, we fix the length of L_2 at 245 nm and adjust the length of L_1, the shorter part of the horizontal resonator, to observe the change of the resonance peaks. When the length of L_1 is adjusted from 190 nm to 205 nm, the resonance peaks of FR5 and FR4 in the transmission spectrum shift slightly from 1313.5 nm to 1327 nm and 1341 nm to 1360 nm, respectively.

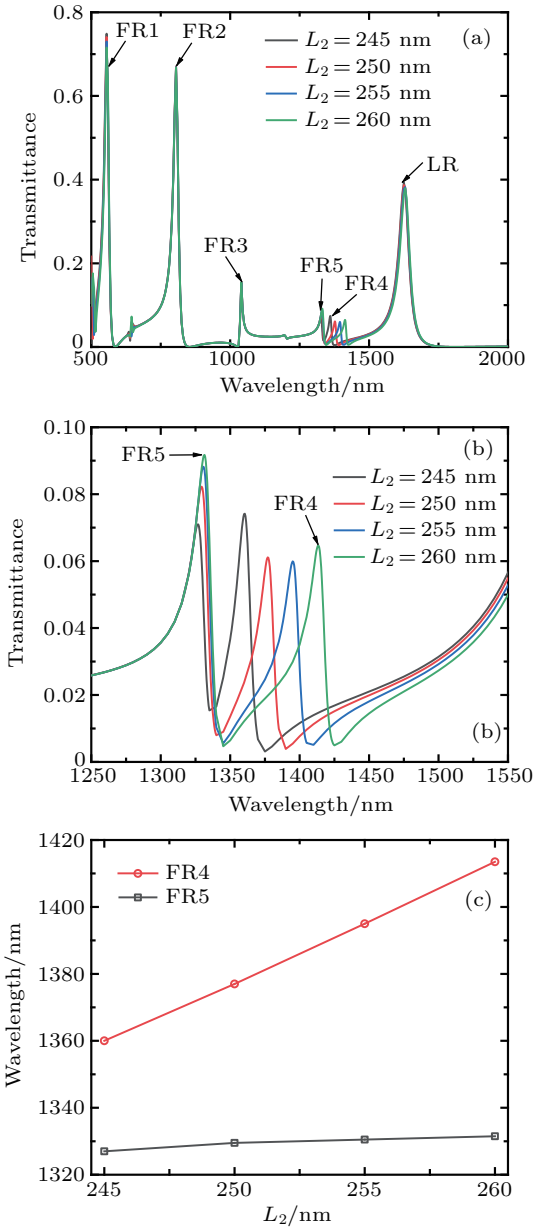


Fig. 13. (a) Transmission spectra of the MIM structure with changing length of the horizontal resonator L_2, (b) transmission spectra of two Fano resonance peaks FR4 and FR5 (wavelength range from 1250 nm to 1550 nm), and (c) resonance wavelengths of two Fano resonance peaks FR4 and FR5 changing with horizontal cavity length L_2.

Then we fix L_1 length at 205 to increase the length of the longer part of the horizontal resonator from 245 nm to 260 nm. From Figs. 13(a) and 13(b), we find that the position of the resonance peak of FR5 hardly changes, while the position of

the resonance peak of FR4 changes uniformly. Thus, we can determine that for the structure of this side-coupled crosshair resonator, the two Fano resonances can be regulated independently by adjusting the length and sides of the horizontal resonator. Figure 13(c) shows the variations of the resonance peaks during the tuning of the horizontal resonator. We obtain that the difference between the resonance peaks of FR5 and FR4 stabilizes when adjusting L_2, the longer part of the horizontal resonator. However, when adjusting L_1, the shorter part of the horizontal resonator, the difference of the resonance peak of FR5 is very stable, but it will slightly affect FR4. This effect can improve the sensitivity of FR4 to incident light frequency, which is what we hope to see.[49]

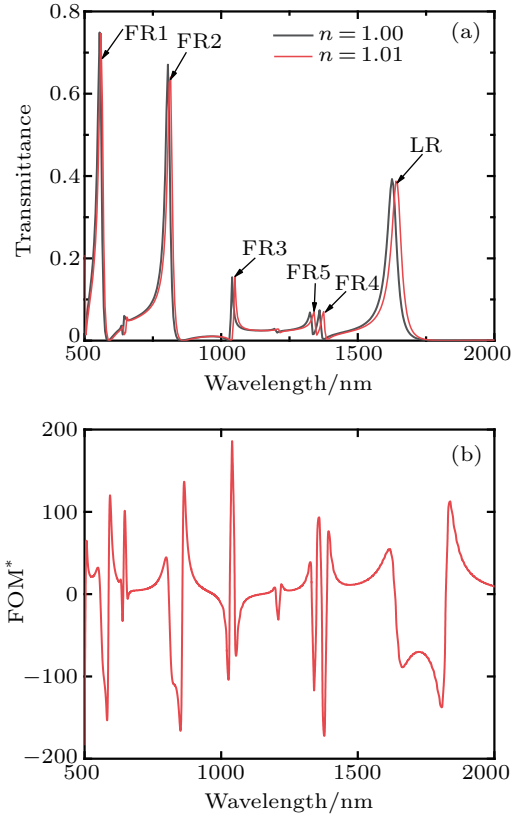


Fig. 14. (a) Transmission spectra with different refractive indexes and (b) FOM* parameter variation with wavelength of the whole system.

The Fano resonance generated by the modified derived structure also has a very small resonance peak difference, so our system is very suitable for making sensors. We change the refractive index of the filling medium in the resonant cavity ($n = 1.00$ and $n = 1.01$), and the change of the transmission spectrum is shown in Fig. 14(a). The refractive index sensitivities of FR1, FR2, FR3, FR4, FR5, and LR are 900 nm/RIU, 800 nm/RIU, 1000 nm/RIU, 1300 nm/RIU, 1300 nm/RIU, 1600 nm/RIU, respectively. The maximum values of these FR sensitivity result 1300 nm/RIU and the sensitivity of LR result 1600 nm/RIU are much larger than 1002 nm/RIU in Ref. [50], 750 nm/RIU in Ref. [51], and 900 nm/RIU in Ref. [6]. This indicates that the system which we designed is very suitable for the sensor. Figure 14(b) shows the FOM* curves at different wavelengths when the refractive index n changes from 1.00 to 1.01. From the figure, we can see that the FOM* values of FR1, FR2, FR3, FR4, FR5, and LR are respectively 136.47, 169.31, 193.00, 183.15, 123.94, and 139.80, which are much higher than the previously reported results.[50–52]

4. Conclusions

In this paper, a single metal baffle MIM waveguide coupled with a semi-circular cavity and a cross-shaped cavity is proposed. When the TM wave is incident into the waveguide structure, the SPPs will be generated at the interface of the MIM. The SPPs form a continuous state on the metal baffle. Meanwhile, the optical signal enters into a semi-circular cavity and a cross-shaped cavity, forming a narrow discrete state. In the near field, the continuous state and the discrete state are coupled to each other to form Fano resonance. It is unable to manufacture the nanoscale materials in our laboratory, and there is no microwave chamber for measuring transmission spectra. So we use the FEM and MICMT to simulate the transmission spectra of this structure and analyze the influence of structural parameters on the refractive index sensing characteristics. There is in good agreement between the two results. Our structure not only is very sensitive to the change of refractive index, but also can realize the independent tuning of Fano resonance peak by changing the structure parameters of semi-circular cavity and cruciform cavity as well as the filling medium. Changing the structural parameters of L_1, L_2, H, g, and t can realize the Fano resonance peak position, the transmission rate, and bandwidth of the effective control, and can also have high sensing performance in the larger regulation range. And the study of the symmetry-breaking features shows that the structure can also produce obvious Fano resonance, and its mechanism makes the arrangement of Fano resonance structure more flexible. After optimizing the structure parameters, the maximum refractive index sensitivity of the device reaches 1600 nm/RIU and the FOM increases up to 193.00. The research results are of significance for guiding us in designing more simple, efficient, and easily machined on-chip highly sensitive micro-nano sensors.

References

[1] Fano U 1961 *Phys. Rev.* **124** 1866
[2] Klimov V V, Pavlov A A, Treshin I V and Zabkov I V 2017 *J. Phys. D: Appl. Phys.* **50** 285101
[3] Ren H, Li X, Zhang Q and Gu M 2016 *Science* **352** 805
[4] Hu F, Yi H and Zhou Z 2011 *Opt. Lett.* **36** 1500
[5] Yang Y R and Guan J F 2016 *Acta Phys. Sin.* **65** 057301 (in Chinese)
[6] Liu C, Fu G, Wang F, Yi Z, Xu C, Yang L and Sun T 2019 *Optik* **196** 163173
[7] Liu J Q, Wang L L, He M D, Huang W Q, Wang D, Zou B S and Wen S 2008 *Opt. Express* **16** 4888
[8] Li J K, Chen Z Q, Yang H, Yi Z, Chen X, Yao W T, Duan T, Wu P H, Li J F and Yi Y G 2020 *Nanomaterials* **10** 257

[9] Wang H Y, Su D, Yang S, Dou X M, Zhu H J, Jiang D S, Ni H Q, Niu Z C, Zhao C L and Sun B Q 2015 *Chin. Phys. Lett.* **32** 107804
[10] Chen Y, Luo P, Tian Y N, Liu X F, Zhao Z Y and Zhu Q G 2017 *Acta Opt. Sin.* **37** 0924002
[11] Li J K, Chen X F, Yi Z, Yang H, Tang Y G, Yi Y, Yao W T, Wang J Q and Yi Y G 2020 *Mater. Today Energy* **16** 100390
[12] Wang Y Y, Chen Z Q, Xu D Y, Yi Z, Chen X F, Chen J, Tang Y J, Wu P H and Yi Y J 2020 *Results Phys.* **16** 102951
[13] Qin F, Chen Z Q, Chen X F, Yi Z, Yao W T, Duan T, Wu P H, Yang H, Li G F and Yi Y G 2020 *Nanomaterials* **10** 207
[14] Qi Y P, Zhang Y, Liu C Q, Zhang T, Zhang B H, Wang L Y, Deng X Y, Bai Y L and Wang X X 2020 *Results Phys.* **16** 103012
[15] Qi Y P, Zhang Y, Liu C Q, Zhang T, Zhang B H, Wang L Y, Deng X Y, Wan X X and Yu Y 2020 *Nanomaterials* **10** 533
[16] Chen J, Wang X X, Tang F, Ye X, Yang L M and Zhang Y B 2020 *Results Phys.* **16** 102867
[17] Wu C C, Guo X D, Hu H, Yang X X and Dai Q 2019 *Acta Phys. Sin.* **68** 148103 (in Chinese)
[18] Tong L, Wei H , Zhang S and Xu H 2014 *Sensors* **14** 7959
[19] Zhang S, Bao K, Halas N J, Xu H and Nordlander P 2011 *Nano Lett.* **11** 1657
[20] Lu H, Liu X, Mao D and Wang G 2012 *Op. Lett.* **37** 3780
[21] Wen K, Hu Y, Chen L Zhou J, Lei L and Meng Z 2016 *Plasmonics* **11** 315
[22] Wu D, Yin J, Tian J P and Yang R C 2018 *J. Quantum Opt.* **24** 55 (in Chinese)
[23] Wu C, Khanikaev A B and Shvets G 2011 *Phys. Rev. Lett.* **106** 107403
[24] Kim J, Soref R and Buchwald W R 2010 *Opt. Express* **18** 17997
[25] Zheng S, Ruan Z, Gao S, Long Y, Li S, He M and Wang J 2017 *Opt. Express* **25** 25655
[26] Qi Y P, Liu C Q, Hu B B, Deng X X and Wang X X 2019 *Results Phys.* **102777**
[27] Fang Y H, Wen K H, Qin Y W, Li Z F and Wu B Y 2019 *Opt. Commun.* **12** 452
[28] Chen J, Fan W, Zhang T, Tang C, Chen X, Wu J and Yu Y 2017 *Opt. Express* **25** 3675
[29] Wu X J, Dou C, Xu W, Zhang G B, Tian R L and Liu H L 2019 *Chin. Phys. B* **28** 014204
[30] Haus H A 1984 *Wave and fields in optoelectronics* (Prentice-Hall) pp. 197–234
[31] Johnson P B and Christy R W 1972 *Phys. Rev. B* **6** 4370
[32] Liu N, Langguth L, Weiss T, Kästel J, Fleischhauer M, Pfau T and Giessen H 2009 *Nat. Mater.* **8** 758
[33] Dionne J A, Sweatlock L A, Atwater H A and Polman A 2006 *Phys. Rev. B* **73** 035407
[34] Zhang Q, Huang X G, Lin X S, Tao J and Jin X P 2009 *Opt. Express* **17** 7549
[35] Hu F, Yi H and Zhou Z 2011 *Opt. Express* **19** 4848
[36] Li S, Wang Y, Jiao R, Wang L, Duan G and Yu L 2017 *Opt. Express* **25** 3525
[37] Shen J, Zhang X M, Li Q L, Wang X Y, Zhao Y J and Jia Y 2019 *Chin. Phys. B* **28** 040503
[38] Wang G, Lu H, Liu X, Mao D and Duan L 2011 *Opt. Express* **19** 3513
[39] Zhong H H, Zhou J H, Gu C J, Wang M, Fang Y T, Xu T and Zhou J 2017 *Chin. Phys. B* **26** 127301
[40] Yang J, Song X, Chen Z, Cui L, Yang S and Yu L 2017 *Plasmonics* **12** 1665
[41] Chen J, Li Z, Zou Y, Deng Z, Xiao J and Gong Q 2013 *Plasmonics* **8** 1627
[42] Huang M, Chen D, Zhang L and Zhou J 2016 *Chin. Phys. B* **25** 057303
[43] Li Z, Wen K, Chen L, Lei L, Zhou J, Zhou D and Wu B 2019 *Appl. Opt.* **58** 4878
[44] Chen Y, Chen L, Wen K, Hu Y and Lin W 2019 *Photon. Nanostruct.-Fundam. Appl.* **100714**
[45] Chen Y, Xu Y M and Cao J G 2019 *Results Phys.* **102420**
[46] Ren X, Ren K and Cai Y 2017 *Appl. Opt.* **56** H1
[47] Liu N, Mesch M, Weiss T, Hentschel M and Giessen H 2010 *Nano Lett.* **10** 2342
[48] Seyyed Hossein, Asadpour G, Solookinejad M, Panahi E and Ahmadi Sangachin 2016 *Chin. Phys. B* **25** 034205
[49] Chen L Y, Tang Z X, Gao J L, Li D Y, Lei C X, Cheng Z Z, Tang S L and Du Y W 2016 *Chin. Phys. B* **25** 113301
[50] Qi Y P, Zhou P Y, Zhang T, Zhang X W, Wang Y, Liu C and Wang X X 2019 *Results Phys.* **14** 102506
[51] Qi Y P, Wang Y, Zhang X W, Liu C, Hu B B, Bai Y L and Wang X X 2019 *Results Phys.* **15** 102495
[52] Wang X X, Zhu J K, Wen X L, Wu X X, Wu Y, Su Y W, Tong H, Qi Y P and Yang H 2019 *Opt. Mater. Express* **9** 3079